

Phase diagram of the vortex system in layered superconductors with strong columnar pinning

Chandan Dasgupta*

*Centre for Condensed Matter Theory, Department of Physics,
Indian Institute of Science, Bangalore 560012, India*

Oriol T. Valls†

*School of Physics and Astronomy and Minnesota Supercomputer Institute,
University of Minnesota, Minneapolis, Minnesota 55455*

(Dated: November 9, 2018)

We present the results of a detailed investigation of the low-temperature properties of the vortex system in strongly anisotropic layered superconductors with a random array of columnar pinning centers. Our method involves numerical minimization of a free energy functional in terms of the time-averaged local vortex density. It yields the detailed vortex density distribution for all local free-energy minima, and therefore allows the computation of any desired correlation function of the time-averaged local vortex density. Results for the phase diagram in the temperature vs. pin concentration plane at constant magnetic induction are presented. We confirm that for very low pin concentrations, the low-temperature phase is a Bragg glass, which melts into an interstitial liquid phase via two first-order steps, separated by a Bose glass phase. At higher concentrations, however, the low-temperature phase is a Bose glass, and the melting transition becomes continuous. The transition is then characterized by the onset of percolation of liquid-like regions across the sample. Inhomogeneous local melting of the Bose glass is found to occur. There is also a depinning crossover between the interstitial liquid and a completely unpinned liquid at higher temperatures. At sufficiently large pin concentrations, the depinning line merges with the Bose glass to interstitial liquid transition. Many of the features we find have been observed experimentally and in simulations. We discuss the implications of our results for future experimental and theoretical work.

PACS numbers: 74.25.Qt, 74.72.Hs, 74.25.Ha, 74.78.Bz

I. INTRODUCTION

Understanding the effects of random pinning on the properties of the mixed phase of high-temperature superconductors (HTSC) and other type-II superconductors is of fundamental importance in the development of a theory of the effects of quenched disorder on the equilibrium and dynamical behavior of a collection of interacting objects (vortex lines or pancake vortices in the case of superconductors in the mixed phase). This subject is also of great practical importance because most applications of HTSCs require a large critical current, which can be achieved only in the presence of effective pinning.

Columnar pinning arising from damage tracks produced by heavy-ion bombardment has received much attention in this context because such extended defects parallel to the direction of the average magnetic flux are very effective^{1,2} in increasing the critical current by localizing vortex lines along their length. Heavy-ion irradiation produces parallel columnar defects, in a random configuration, each of which can trap one or more vortex lines at low temperatures. The effects of an array of such extended defects, oriented perpendicular to the superconducting layers, on the properties of the mixed phase of HTSCs in a magnetic field perpendicular to the layers have been extensively studied experimentally^{1,2,3,4,5,6,7,8}, theoretically^{9,10,11,12}, and numerically^{13,14,15,16}. In the regime in which the areal concen-

tration of randomly placed columnar pins exceeds that of vortex lines (as determined by the value of the magnetic induction B) the behavior of this system is now fairly well-understood. Theoretical studies^{9,11} based on a mapping of the thermodynamics of the system to the quantum mechanical properties of a two-dimensional system of interacting bosons in a random potential, as well as experimental^{3,4} studies, have established that in this regime the system undergoes a continuous phase transition between a low-temperature “strong” Bose glass (BoG) phase and a high-temperature vortex liquid phase. In the “strong” BoG phase nearly all the vortex lines are strongly pinned at columnar defects and both translational and bond-orientational correlations of the vortex lines are short-range, indicating a strongly disordered structure.

The behavior of the system in the “dilute pin” regime, where the number of columnar pins is much smaller than the number of vortex lines, is much less well understood. Several years ago, it was pointed out by Radzihovsky¹⁰ that in this regime the system may exhibit a first-order transition between a low-temperature “weak” BoG and a high-temperature vortex liquid. In the “weak” BoG phase only a fraction of vortex lines are strongly pinned at the columnar defects, and the remaining vortex lines are weakly pinned in the interstitial region between defects. The liquid phase into which the “weak” BoG melts upon increasing the temperature is expected to have a mixed character in the sense that some of the vortices

remain pinned at the pinning centers, while the other, interstitial ones form a liquid. This partially pinned interstitial liquid (IL) should then exhibit a crossover to a completely depinned vortex liquid at a higher temperature. This behavior is also suggested in a recent theoretical study¹² based on the analogy of the vortex system with a two-dimensional system of bosons in a random potential.

Recent experiments^{6,7,8} on the highly anisotropic, layered HTSC $\text{Bi}_2\text{Sr}_2\text{CaCu}_2\text{O}_{8+x}$ (BSCCO) with a small concentration of randomly placed columnar pins perpendicular to the layers have provided many interesting results, some of which are in agreement with the theoretical predictions mentioned above. These experiments were carried out for different values of the relative pin concentration c , ($c = N_p/N_v \equiv B_\phi/B$, where N_p is the number of columnar pins, N_v the number of vortex lines and B_ϕ the “matching field”). For small values of c , the experiments indicate a first-order phase transition between a high-temperature vortex liquid and a low-temperature BoG phase in which the vortices are arranged in a polycrystalline structure with grain boundaries separating crystalline regions of different orientations. The temperature at which this transition occurs remains close to the melting temperature of the vortex lattice in samples without columnar pins, if the value of c is sufficiently small. As c is increased while keeping B (and hence the density of vortex lines) constant, the transition temperature begins to increase. This is in agreement with theoretical predictions¹⁷. As c is increased further, the nature of the transition changes from first-order to continuous. For small values of c , the liquid into which the BoG melts has the “mixed” character mentioned above – it is called vortex “nanoliquid” in Ref. 8. This partially pinned interstitial liquid undergoes a crossover to a fully depinned vortex liquid as the temperature is increased further. The temperature at which this crossover occurs is found to be nearly independent of the pin concentration, whereas the melting temperature of the BoG phase increases with increasing c . Therefore, the temperature range over which the interstitial vortex liquid exists becomes narrower with increasing c , and eventually goes to zero. Thus, for sufficiently high values of c , the BoG melts directly into a liquid in which all the vortices are delocalized.

Some of the characteristic features found in the experiments mentioned above have been reproduced in simulations of a collection of interacting vortex lines in the presence of a random array of columnar pins. These include the polycrystalline nature of the low-temperature BoG phase¹⁴, the increase of its melting temperature with increasing pin concentration for strong columnar pins¹⁵, and the occurrence of an interstitial liquid phase for low values of c ¹⁶. The simulations of Ref. 16 have also provided evidence for the existence of an additional phase, a topologically ordered Bragg glass (BrG)¹⁸, at low temperatures in systems with a small concentration of weak columnar pins.

Assuming the magnetic field to be perpendicular to the layers, the vortex lines in highly anisotropic layered HTSCs may be thought of as stacks of pancake vortices localized on the superconducting layers. These pancake vortices constitute a system of pointlike objects that interact among themselves and also with a potential, external to them, arising from the pinning centers. We have recently performed a study^{19,20} of the thermodynamic and structural properties of such a system, with a very small concentration of randomly distributed, strong, columnar pins perpendicular to the layers. We used a density functional theory, based on the Ramakrishnan-Yussouff free energy functional²¹, to analyze the structure and equilibrium properties of this classical system of pointlike objects. In this method the free energy is expressed as a functional of the time-averaged local density of the pancake vortices. Different local minima of the free energy represent different possible phases of the system in this mean-field description. A numerical minimization procedure locates the various minima of the free energy functional. The phase diagram of the system in the relevant parameter space was then mapped out by locating the points where the free energies of different minima cross.

There are three distinct phases for very small values ($c \leq 1/64$) of the pin concentration: a topologically ordered BrG phase²², a polycrystalline BoG phase, and an IL phase with coexistence of localized and mobile vortices. The BrG is the equilibrium phase at low temperatures at these small values of c . As the temperature T is increased, this phase melts into the IL in *two steps* – the BrG and IL phases are separated by a small region of the BoG phase. Both the BrG-to-BoG transition and the BoG-to-IL transition which occurs at a slightly higher T were found to be first-order, indicating a two-step first-order melting of the nearly crystalline, topologically ordered BrG phase. Experimentally observed spatial variations of a “local” transition temperature^{6,23} were also reproduced.

In this paper, we present the results of our investigation of the behavior of the same system for larger values of the pin concentration, thereby generating the phase diagram in the entire relevant area of the T - c plane. The methods used in this study are the same as those used^{19,20} for the small- c regime. The objective here is to connect the behavior found for small c with the well-known results (continuous transition between a low-temperature BoG phase and a high-temperature depinned vortex liquid) for large c . Another motivation is to provide an understanding of some of the experimental observations mentioned above.

The main results of our present study are as follows. We find that the width (in temperature) of the intermediate BoG phase that separates the low-temperature BrG and high-temperature IL phases increases initially as the pin concentration c is increased from a very small value at fixed B . As c is increased further, the BrG minimum of the free energy ceases to be the one with the

lowest free energy at low temperatures. This observation indicates that the BoG phase is thermodynamically stable only if the pin concentration is smaller than a critical value. This critical value of c turns out to be close to $1/32$ for the system parameters (appropriate for BSCCO) used in our calculation, at $B = 2\text{kG}$. For higher values of c , we find a low-temperature polycrystalline BoG phase and a high-temperature IL phase. The transition between these two phases becomes continuous as the value of c is increased. A continuous transition is difficult to locate in a mean-field calculation. In that case the minimum representing the low-temperature BoG phase transforms continuously into that corresponding to the high-temperature IL phase as the temperature is increased: there is no free-energy crossing that can be used to define the transition temperature. Indeed, it becomes difficult to distinguish a true continuous transition from a crossover. Guided by existing theoretical and experimental results (summarized above), we assume that there is a continuous transition, and then locate the transition temperature using a criterion based on *the occurrence of percolation of liquid-like regions across the sample*. The transition temperature obtained from this definition was found^{19,20,24} at lower c to coincide with that obtained from free energy crossings. The details are explained in Sec. III below. In a study²⁵ of the two-dimensional disordered bosonic Hubbard model, it was found that the transition between the BoG and superfluid phases nearly coincides with the onset of percolation of sites that have large values of the superfluid order parameter. Since the system we are considering can be mapped approximately to a two-dimensional system of interacting bosons in a random potential, we believe that the percolation-based criterion we have used to determine the transition temperature is quite reasonable.

The BoG–IL transition temperature obtained this way increases slightly as the pin concentration is increased at fixed B . The BoG phase continues to exhibit a polycrystalline structure as c is increased: the typical size of crystalline domains decreases with increasing c . To estimate the depinning temperature, we monitor the average value of the integrated density of pancake vortices inside the range of the pinning potential of each columnar defect. This quantity decreases as the temperature is increased. We define the depinning temperature as that at which the integrated density falls below an appropriately chosen critical value. The depinning temperature obtained this way decreases slowly with increasing c . This happens because^{24,26} two pinning centers can not be simultaneously occupied by vortices if they happen to be very close to each other. This effect reduces the average pinning efficiency of a defect as c is increased. For the range of c we have considered ($c \leq 1/8$), the depinning temperature is found to lie above the temperature at which the BoG phase transforms into a liquid. So, for these values of the pin concentration, the liquid phase into which the BoG melts can be classified as IL, with a coexistence of pinned and delocalized vortices. Our

results indicate that the IL would disappear (the BoG would melt into a depinned liquid) at a value of c just slightly higher than $1/8$. From that point on, there would be a single transition between the low-temperature BoG and a high-temperature depinned vortex liquid: thus our work encompasses all the interesting parts of the phase diagram in the c vs. T plane. Using a criterion based on the degree of localization of the vortices, we define a local transition temperature and find that this temperature exhibits spatial variations similar to those found in experiments^{6,23}.

The rest of this paper is organized as follows. In section II, we describe the model and the computational method used in our study. The main results obtained in this work are presented and discussed in detail in section III. The last section IV contains a summary of our main results and a few concluding remarks.

II. METHOD

The general method used in this study has been described previously^{20,24} and we will keep the discussion here to the minimum necessary to establish notation. We consider the limit of highly anisotropic layered superconductors with vanishing interlayer Josephson coupling. In this limit, the energy of a system of pancake vortices can be written as a sum over anisotropic pair-wise interactions. This limit is appropriate to HTSCs of the Tl and Bi families. We will use material parameters appropriate to BSCCO throughout this work.

The pinning potential due to a collection of columnar pins perpendicular to the layers is the same on all the layers. This implies that the time-averaged local density $\rho(\mathbf{r})$ (\mathbf{r} is a two-dimensional vector denoting the position on a layer) of pancake vortices is also the same on all the layers. This makes the problem effectively two-dimensional^{20,24}. We conduct a numerical search for local and global minima of the free energy F written as a functional of $\rho(\mathbf{r})$:

$$F[\rho] - F_0 = F_{RY}[\rho] + F_p[\rho]. \quad (2.1)$$

Here F_0 denotes the free energy of a uniform vortex liquid of density $\rho_0 = B/\Phi_0$, with B being the magnetic induction and Φ_0 the superconducting flux quantum. In the absence of pinning, the free energy functional is given by the Ramakrishnan-Yussouff²¹ expression:

$$\begin{aligned} \beta F_{RY}[\rho] = & \int d^2r [\rho(\mathbf{r})\{\ln(\rho(\mathbf{r})) - \ln(\rho_0)\} - \delta\rho(\mathbf{r})] \\ & - \frac{1}{2} \int d^2r \int d^2r' \tilde{C}(|\mathbf{r} - \mathbf{r}'|) \delta\rho(\mathbf{r}) \delta\rho(\mathbf{r}') \end{aligned} \quad (2.2)$$

where β is the inverse temperature, $\delta\rho(\mathbf{r}) \equiv \rho(\mathbf{r}) - \rho_0$ the deviation of the density from the uniform value, and $\tilde{C}(r)$ a direct pair correlation function²⁷, for which we use the hypernetted chain²⁸ results. With these assumptions, the

results depend on the in-plane London penetration depth $\lambda(T)$ and on the dimensionless parameter Γ given by:

$$\Gamma = \beta d \Phi_0^2 / 8\pi^2 \lambda^2(T). \quad (2.3)$$

We take $d = 15\text{\AA}$ for the interlayer distance in BSSCO, and the standard two-fluid form for $\lambda(T)$ with $\lambda(0) = 1500\text{\AA}$ and $T_c = 85\text{K}$ (at zero field).

The remaining term in the right-hand side of Eq.(2.1) represents the pinning and is of the form:

$$F_p[\rho] = \int d^2r V_p(\mathbf{r}) \delta\rho(\mathbf{r}). \quad (2.4)$$

where the pinning potential V_p is written as a sum extending over the positions of the pinning columns in the transverse plane:

$$V_p(\mathbf{r}) = \sum_j V_0(|\mathbf{r} - \mathbf{R}_j|). \quad (2.5)$$

The potential V_0 corresponding to a single pinning center is chosen to be of the usual truncated parabolic form²⁶

$$\beta V_0(r) = -\alpha\Gamma[1 - (r/r_0)^2]\Theta(r_0 - r). \quad (2.6)$$

We use the quantity a_0 defined by $\pi\rho_0 a_0^2 = 1$ as our unit of length. In terms of this quantity, we take $r_0 = 0.1a_0$. As for the dimensionless strength α , we use $\alpha = 0.05$. For this combination of values²⁴ each pinning center traps nearly one vortex in the lower part of the temperature range studied.

The minima of the free energy are found by discretizing the density over a computational triangular lattice of spacing h . The value of h is chosen to be sufficiently small to provide an accurate description of the spatial variations of $\rho(\mathbf{r})$. The set of discretized variables $\{\rho_i\}$ is given by $\rho_i \equiv \rho(\mathbf{r}_i)\sqrt{3}h^2/2$, where $\{\mathbf{r}_i\}$ represents the set of computational lattice points. One then minimizes the free energy with respect to the $\{\rho_i\}$ set by using a procedure²⁹ that ensures that the nonnegativity constraint on these variables is satisfied.

III. RESULTS

Using the methods described above, we have studied relative pin concentrations c ($c = N_p/N_v$ as defined above) ranging from $c = 1/32$ to $c = 1/8$, keeping B fixed at 2 kG. Results for smaller concentrations have been previously^{19,20} reported. All results reported here are for a computational lattice size $N = 1024$ and the computational lattice spacing is $h = a/16$ where $a = 1.998a_0$ is²⁴ the equilibrium lattice constant of the Abrikosov vortex lattice in the absence of pinning in the temperature range considered (see below) which is chiefly determined by the melting temperature of the unpinned vortex lattice, namely $T_m^0 \approx 18.4\text{K}$ at the field studied. For these

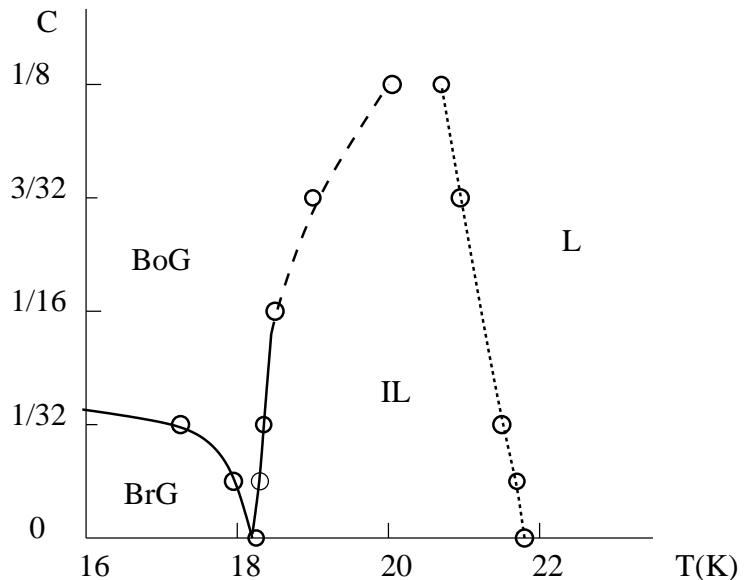


FIG. 1: The temperature, T , vs relative pin concentration, c , phase diagram obtained from our results for $B = 2\text{kG}$. The labels L, IL, BoG and BrG denote liquid, interstitial liquid, Bose glass and Bragg glass phases, respectively. Open circles represent actual data points, and the lines are guides to the eye. The solid lines indicate first-order transitions, the dashed line, continuous transitions, while the dotted line marks the location of the depinning crossover. See text for details.

values of h and N the system contains $N_v = 4096$ vortices and therefore the number of pins ranges from $N_p = 128$ to $N_p = 512$. These pins are set at random positions. The results are very consistent from sample to sample and it turns out to be sufficient to average over five such samples.

The initial conditions used for the variables ρ_i to start the minimization process are of two kinds: the first kind is “liquid-like” with uniform density, and the second is a “crystal-like” initial state with values of the ρ_i variables obtained, for a given random pin configuration, by minimizing the pinning energy with respect to all the possible crystal configurations related by symmetry operations of the triangular lattice. The first kind of initial conditions leads, if one quenches to a sufficiently high temperature (higher than T_m^0), to free energy minima which correspond to a liquid state, as revealed by the methods of analysis discussed below. The second kind leads²⁰ to a BrG state if quenched to a sufficiently low T provided (as we shall see) that c is not too high. BoG states can be obtained by slowly (we typically use 0.2K temperature increments) cooling liquid states obtained as described above, or by quenching to sufficiently low T either with the first kind of initial conditions or with the second kind at higher c , as we shall see below.

From the set of $\{\rho_i\}$ values obtained at each minimum one can calculate the density correlations, such as the

structure factor $S(\mathbf{k})$:

$$S(\mathbf{k}) = |\rho(\mathbf{k})|^2 / N_v \quad (3.1)$$

where $\rho(\mathbf{k})$ is the discrete Fourier transform of the $\{\rho_i\}$. Equivalently, one can consider the real-space correlations through the discrete Fourier transform of $S(\mathbf{k})$, which is the two-point spatial correlation function $g(\mathbf{r})$ of the time-averaged local density. It is also useful to consider the angularly averaged counterparts of these two quantities, which we will call $S(k)$ and $g(r)$ respectively.

However, evaluating this and other correlations is not all one can do: one can use the set $\{\rho_i\}$ to directly visualize the density distribution. Further, one can examine the structure formed by the *vortices* themselves. To do so, one extracts from the $\{\rho_i\}$ variables the local peak densities: we define site i as being a local peak location if ρ_i is larger than any value of ρ_j evaluated at a site j within a radius $a/2$ from i , where a is the lattice constant of the vortex lattice in the absence of pinning. We refer to the network formed by these peak locations as the “vortex lattice”. At low temperatures, the number of peaks matches the number of vortices N_v , indicating that, as expected, the vortices are localized. This “vortex lattice” can be studied by direct visualization, and also by carrying out a Voronoi construction for it, that is, by examining its defect structure.

To describe orientational order, we will also study the bond-orientational correlation function $g_6(r)$ in the vortex lattice which we define as:

$$g_6(r) = \langle \psi(\mathbf{r})\psi(0) \rangle \quad (3.2a)$$

where $\langle \dots \rangle$ brackets denote average over the vortex lattice and the field $\psi(\mathbf{r})$ is:

$$\psi(\mathbf{r}) = \frac{1}{n_n} \sum_{j=1}^{n_n} \exp[6i\theta_j(\mathbf{r})] \quad (3.2b)$$

where $\theta_j(\mathbf{r})$ is the angle made by the bond connecting a vortex at \mathbf{r} to its j -th neighbor and a fixed axis, and n_n is the number of neighbors of the vortex at \mathbf{r} , as determined from a Voronoi construction.

Quite analogously, one can define a “translational correlation function” $g_G(r)$ of the vortex lattice by an equation identical to the right-hand side of Eq. (3.2a), but with the field ψ replaced by

$$\psi_G(\mathbf{r}) = \exp(i\mathbf{G} \cdot \mathbf{r}) \quad (3.3)$$

where \mathbf{G} is one of the shortest nonzero reciprocal lattice vectors of the triangular vortex lattice in the absence of pinning. We will average over the six equivalent \mathbf{G} 's.

Different free energy minima at a given temperature are found, as in previous work^{19,20} by starting the minimization program with different initial conditions, either in a quenching mode, where the initial conditions are liquid-like or crystal-like, or on a warm-up (or cool-down) mode where the density values for a certain minimum are used as input to find a similar minimum at

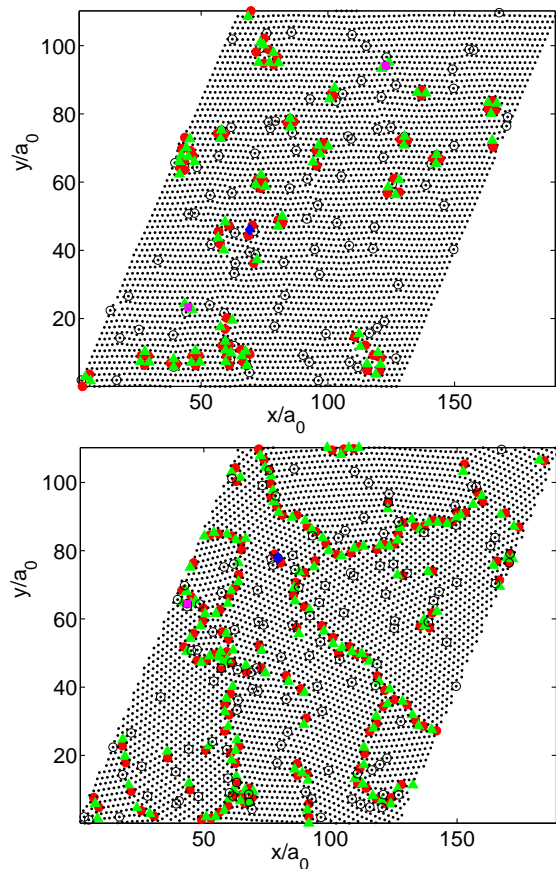


FIG. 2: (Color online) Voronoi plots for the BrG (left) and BoG (right) states found at $T = 17\text{K}$ for one of the samples with $c = 1/32$. The black dots denote sites with six neighbors, the (red) solid circles label fivefold coordinated sites, and the (green) triangles sevenfold coordinated sites. A few occurrences of fourfold and eightfold coordinated sites are indicated by (magenta) squares and (blue) diamonds, respectively. Sites surrounded by black circles are where pinning centers are located.

a slightly higher (or lower) temperature. Determination of the nature of a given free energy minimum is carried out by careful consideration of all the information obtained, both in the original computational lattice and on the vortex lattice.

A. Phase diagram

We start the discussion of our results by summarizing the phase diagram we obtain in Fig. 1. The data which lead to this diagram and results supporting it will be discussed in the rest of this section. The results shown are for a fixed value of the magnetic induction, $B = 2\text{kG}$. We see in Fig. 1 that at small concentrations c of random pins, and low T , one has a nearly crystalline, topologically ordered BrG phase which, upon warming, melts into an IL in two first-order steps, indicated by solid lines. As already seen in Refs. 19 and 20 for $c \leq 1/64$, the low- T

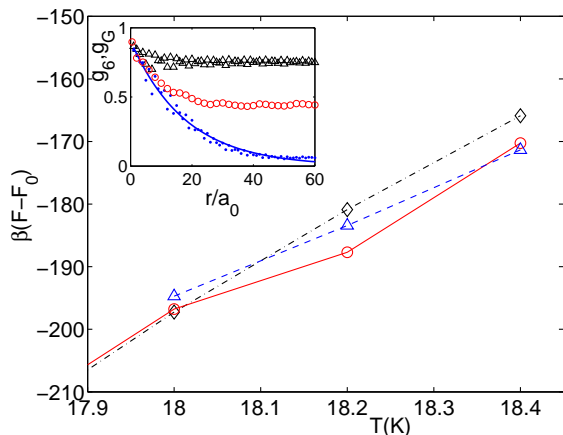


FIG. 3: (Color online) The main plot shows the free energies as a function of T for three states obtained for the same sample as in Fig. 2, displaying the first-order transitions at the crossings. The symbols represent the data points, joined by straight segments. (Black) diamonds and dash-dotted line: BrG. (Red) circles and solid line: BoG. (Blue) triangles and dashed line: IL. In the inset, several correlation functions are plotted versus dimensionless distance, all at $T = 17\text{K}$ and averaged over five configurations: the correlation function $g_6(r)$ (Eq. (3.2a)) is shown for the BrG ((black) triangles) and the BoG ((blue) dots) states, with the solid curve being an exponential fit to the dots. The (red) open circles represent the data for the function $g_G(r)$ (Eq. (3.3)) for the BrG state.

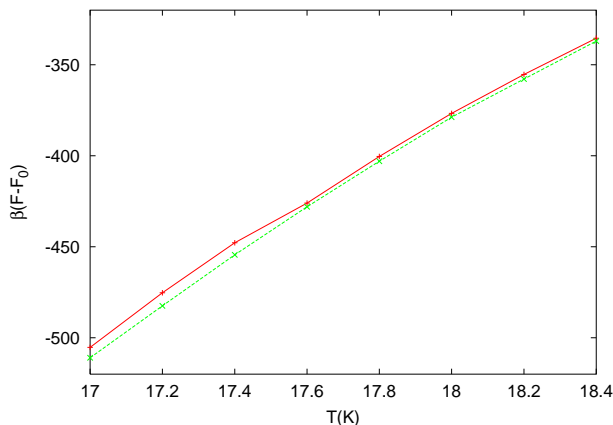


FIG. 4: (Color online) Free energy (in units of $k_B T$) of two different states at a concentration $c = 1/16$, as a function of temperature. The (red) plus signs and solid line correspond to a state obtained by quenching to $T = 17\text{K}$ with crystalline initial conditions and then slowly warming. At concentrations $c \leq 1/32$ this produces a BrG state. The (green) crosses and dashed line correspond to a state similarly obtained but by starting with uniform initial conditions. This state is BoG-like at all c values. One can see that the attempted BrG state has, at this concentration, a higher free energy, with the difference actually increasing at low T .

BrG phase and the higher T IL are separated by a sliver of polycrystalline BoG phase. We find here that, as one increases c , the temperature region where the intermediate BoG occurs first becomes wider. However, as c exceeds $1/32$, the BrG drops out of the picture: the free energy of any phase that may be identified as BrG-like becomes, as we shall see, too high, and the only transition is between the IL and a BoG phase. This transition is, furthermore, not first-order but continuous (dashed line). The transition line bends markedly towards higher temperatures as c increases. We have indicated also in the figure (dotted line) the depinning crossover, determined as explained below, which indicates the temperature at which the pins are no longer able to effectively pin the vortices. This line, which separates the IL from the ordinary vortex liquid, is weakly T dependent, and very near the highest c studied, it merges with the IL to BoG line, indicating that, from that point on, the phase diagram becomes very simple, as only a single transition between an unpinned liquid phase and a pinned BoG phase occurs.

B. Results for $c = 1/32$

We begin by considering the concentration $c = 1/32$. All of our results are obtained on a computational lattice of size $N = 1024$ so that, with the value of h chosen as discussed above, we always have $N_v = 4096$ vortices. Therefore at this concentration we have $N_p = 128$ pins. We can obtain at this concentration three kinds of states: the first kind is obtained by quenching the system to a rather low T with crystalline initial conditions. An example (discussed in more detail below) is shown in the left panel of Fig. 2 which depicts the vortex lattice structure (positions of local density peaks). The second kind is obtained by quenching to similar temperatures with liquid-like initial conditions. An example is shown in the right panel of the same figure. Finally, if one quenches with liquid initial conditions to a high temperature (e.g. $T = 18.6\text{K}$), one obtains a third state which is very obviously liquid-like. This is as previously²⁰ found for $c = 1/64$.

We show in Fig. 2 Voronoi plots for the vortex lattice at $T = 17.0\text{K}$. These plots show the defect structure of the two different kinds of low temperature states. One can see in the left plot a nearly crystalline structure, with defects localized and consisting of paired dislocations and larger clusters of tightly bound dislocations with net Burgers vector equal to zero. The second plot is quite different: there are many more defects and they are not randomly distributed, but they are organized forming continuous grain boundaries which give the sample an overall “polycrystalline” structure. Therefore, one is led to identify the first state as the BrG, and the second, as the BoG. Examination of the correlation functions confirms that this situation is in all ways identical to that previously found²⁰ at smaller values of c . For this reason,

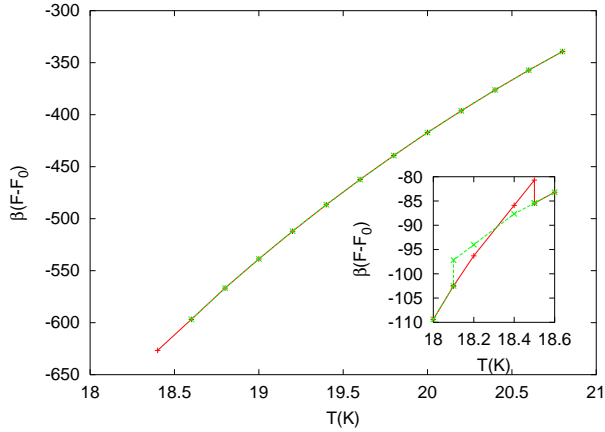


FIG. 5: (Color online) Main figure: The dimensionless free energy for a concentration $c = 1/8$. The (red) plus signs and (green) crosses represent results obtained on warming and cooling respectively. They are so similar that the symbols merge into an apparent asterisk. In the inset the results of a similar cycling at $c = 1/64$ are shown, with the same symbols: clearly now a hysteretic first-order transition occurs.

many of the details will not be repeated here.

The free energy analysis for this sample is shown in the main plot of Fig. 3. The data for the BoG and BrG states were obtained by warming up the states shown in Fig. 2, while the IL state data were obtained from cooling the high- T liquid. This IL state becomes unstable if one attempts to cool it further; similarly, the two solid states found at low temperatures eventually melt if warmed up enough. Here one can see that the IL state transforms, upon lowering T , to the BoG state via a first-order transition, while, upon further cooling, there is a second transition to the BrG. For this sample, the spread between the two transitions is about 0.4K but this number is rather variable from sample to sample. The average is represented in Fig. 1. There is a very clear increase in the width of this interval, compared to that for $c = 1/64$.

The results shown in the inset in Fig. 3 confirm our identification of the low- T phases. Here, different correlation functions are plotted versus distance measured in units of a_0 . These are for $T = 17\text{K}$ and represent averages over five configurations. For the BrG state we plot the bond-orientational correlation function $g_6(r)$ (Eq. (3.2a)), [(black) triangles] and also the translational correlation function $g_G(r)$ defined in Eq. (3.3) [(red) open circles]. It can be seen that $g_6(r)$ exhibits long-range order, and that the decay of $g_G(r)$ at long distances is much slower than the initial exponential decay. The remaining data points [(blue) dots] show $g_6(r)$ for the BoG state. In this case, there is no long-range order: the solid curve is an exponential fit to the data. These results are quite consistent with the defect structures found in the Voronoi plots.

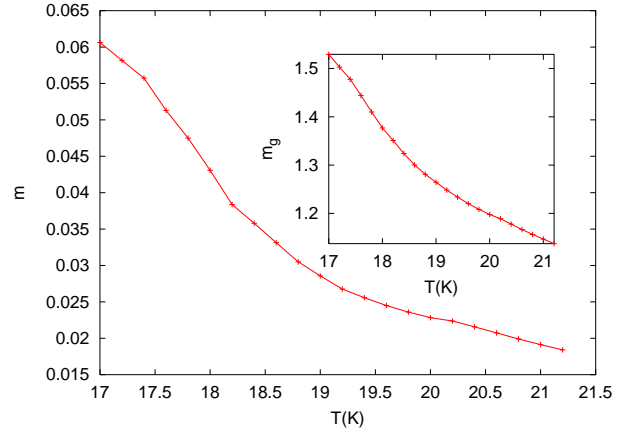


FIG. 6: (Color online) Degree of translational order, measured in two different ways, as a function of temperature at $c = 3/32$. In the main plot, the “order parameter” m obtained from the structure factor (see Eq.(3.4)) is plotted, while in the inset the height of the first peak at finite r in $g(r)$ is displayed. In all cases the symbols are data points joined by straight segments.

C. Results for $c > 1/32$

The behavior described above changes, however, when c is increased above the value of $1/32$. In Fig. 4 we have shown some free energy results (in units of $k_B T$) obtained at $c = 1/16$. Results are shown, for the same pin configuration, for two states both obtained by quenching to $T = 17.0\text{K}$ and then warming up. One of the states [(red) plus signs and solid line] is obtained from crystal-like initial conditions, while for the other set of data [(green) crosses and dashed line], the initial conditions are liquid-like. At smaller c , the state obtained from crystal-like initial conditions is BrG-like and is the lowest free-energy state at low T , while the other state is a BoG, and is the lowest free-energy state at temperatures close to melting. This is not the case here: the state obtained from liquid-like initial conditions is in fact a BoG, but the putative BrG (which is rather more disordered than the BrG states found for smaller values of c) turns out to have a higher free energy than the BoG, and the difference becomes larger at lower T . There is therefore no longer a transition between the BoG and BrG states. At higher values of c , the same situation obtains, except that the difference in free energies between the states obtained using the two different initial conditions becomes larger. Also, the minima obtained from crystal-like initial conditions begin to exhibit unpaired dislocations, so that they can no longer be convincingly identified as BrG. This indicates that the BoG to BrG first-order transition line turns over near $c = 1/32$ as indicated in the phase diagram of Fig. 1.

We will therefore from now on ignore the BrG-like state at these larger values of c , since it is never the equilibrium state. The nature of the remaining transition, from

IL to BoG, also changes in this concentration range: it becomes a continuous transition. This can be seen in the main part of Fig. 5, where we plot the dimensionless free energy as a function of T for a pin configuration with $c = 1/8$. The BoG state obtained in the usual way by quenching to low T is warmed up, [(red) plus signs and solid line] and then cooled down again [(green) crosses, dashed line]. The values of the free energy obtained in the heating and cooling runs are the same within numerical error: this is made evident by the symbols merging into each other and forming (bi-colored) asterisks. This behavior is in contrast with that found at lower c , as exemplified in the inset of Fig. 5, which is for a system subjected to similar temperature cycling at $c = 1/64$. In that case one can see the obvious hysteresis associated with the first-order transition between BoG and IL (the transition to BrG at a lower temperature is not shown in this plot). Plots similar to those in Figs. 4 and the main plot of Fig. 5 can be obtained for any pin configuration with $c \geq 1/16$. Thus, there is only one transition in this higher concentration range and it is, furthermore, continuous. Further evidence for this, and more details on this transition are shown in the next few figures.

In Fig. 6 we give an example of the behavior of the degree of translational order in the system, as a function of T , at a concentration $c = 3/32$. Two different measures of the degree of translational order are plotted. One, displayed in the main plot, is the value of an “order parameter” m obtained from the structure factor $S(\mathbf{k})$. It is defined as

$$m \equiv \sqrt{S_{max}/N_v}, \quad (3.4)$$

where S_{max} is the largest value of $S(\mathbf{k})$ averaged over the six \mathbf{k} vectors related to one another by lattice symmetry. This is the more traditional measure of the degree of translational order: m would be equal to unity for a perfect lattice. The data points represent averages over five configurations and are obtained by initially quenching the system to $T = 17\text{K}$ with liquid-like initial conditions, and then warming up. Clearly, no sharp change in the value of the quantity plotted occurs, even though it changes by a factor of three in the T range considered. In the inset, we plot the value m_g of the first maximum at finite r of the angularly averaged correlation function $g(r)$. The behavior is qualitatively similar, and again shows no evidence of any discontinuity, even beyond the temperature where the system is expected to melt and where, as we shall see below, the system is in fact in an IL state. This is in contrast with the discontinuous changes in the order parameter found upon melting at lower c (see e.g. Fig. 6 in Ref. 20). The plots in Fig. 6 exhibit largest slopes near $T \sim 18.5\text{K}$, suggesting that a continuous transition (or a crossover) takes place near this temperature.

We next visualize the phases involved as a function of T and c through Voronoi and peak-density plots for the vortex lattice. As explained above, we consider only the states obtained from liquid-like initial conditions. As shown in Fig. 5, these states can be warmed up and

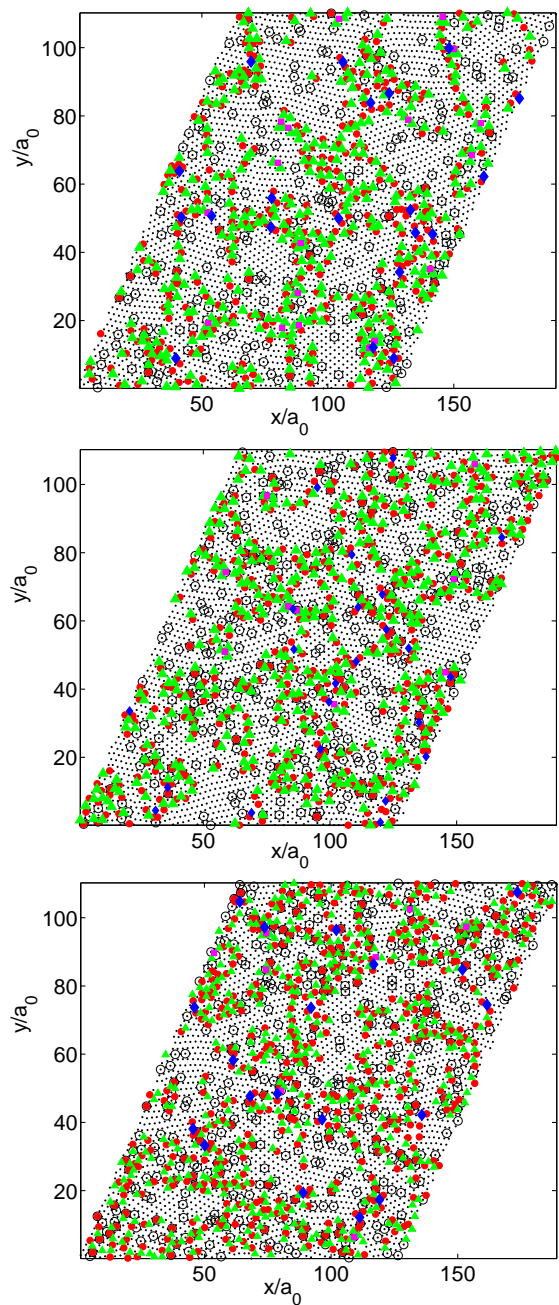


FIG. 7: (Color online) Voronoi plots for samples with $c = 1/16$, $c = 3/32$, and $c = 1/8$ (from top left to bottom) at $T = 18.4\text{K}$. The meaning of the symbols is the same as in Fig. 2.

cooled down reversibly. In Fig. 7 we show Voronoi plots, all at the same temperature $T = 18.4\text{K}$, for three concentrations, ranging from $1/16$ to $1/8$. The temperature chosen is slightly to the left of the dashed transition line in Fig. 1: the plots still show BoG character. As one can see, the nature of the state does not change with pin concentration, except that the number of defects obviously increases. The crystalline domains are still quite well defined, but they become smaller as c increases. Our

results for the dependence of the number of defects on c are consistent with this number being proportional to \sqrt{c} . This implies that the number of crystalline domains in the BoG state is proportional to c . This being so, the area of a typical crystalline grain would be proportional to $1/c$, and the length of its perimeter to $1/\sqrt{c}$. Hence, the total length of the grain boundaries in the sample (which is approximately proportional to the number of dislocations since nearly all the dislocations appear at grain boundaries) would be proportional to \sqrt{c} . This is similar to the experimental results reported in Ref. 7.

This result suggests a simple qualitative explanation for the appearance of the BrG phase at very small values of c and its subsequent disappearance. The elastic energy cost for the formation of the grain boundaries in the BoG phase should be proportional to the total length of the grain boundaries, i.e. to \sqrt{c} , neglecting the contribution from interactions between grain boundaries for small c . The pinning energy is minimized in the BoG phase by having essentially all pinning centers occupied by vortices in this phase (see section III D below). The free energy cost of forming the BrG state arises from two sources: First its pinning energy is higher because pinning centers that lie far away from any lattice point of the crystalline initial state used for obtaining a BrG minimum are not fully occupied by vortices (a similar behavior was found in the simulation of Ref.16). Second, there is extra elastic energy associated with the formation of the defect clusters with zero net Burgers vector. These defect clusters, found mostly near pinning centers, are formed as the effect of the randomly located pinning centers is accommodated in the initial crystalline structure by small displacements of the vortices from their ideal lattice positions towards the nearest pinning center. These “uncharged” defect clusters, called “twisted bond defects”³⁰, cost relatively little energy because they can be formed by distorting the lattice at short range. The energy cost of forming these defect clusters is proportional to their number at the relevant small c values. Our numerical results for the c -dependence of the number of unoccupied (or partially occupied) pinning centers and the number of dislocations in the BrG state suggest that the energy cost arising from both these sources is proportional to the defect concentration c . Since \sqrt{c} grows faster than c as c is increased from zero, the BrG phase would be favored over the BoG phase at very small values of c , but not at higher ones, as found in our study.

The same $c = 1/16$ configuration studied in the top left panel of Fig. 7 is examined in Fig. 8 as a function of the temperature. In this case we show plots of the vortex density at the local density peaks, rather than Voronoi plots, at three values of T , $T = 17.6\text{K}$, 18.4K and 19.2K . The values ρ_{peak} of the density at the local density peaks, normalized to ρ_0 , are shown according to the symbol (and color) scheme explained in the caption. Higher values of the peak density indicate strongly localized, solid-like behavior, while lower values indicate that the corresponding vortices are more delocalized, as

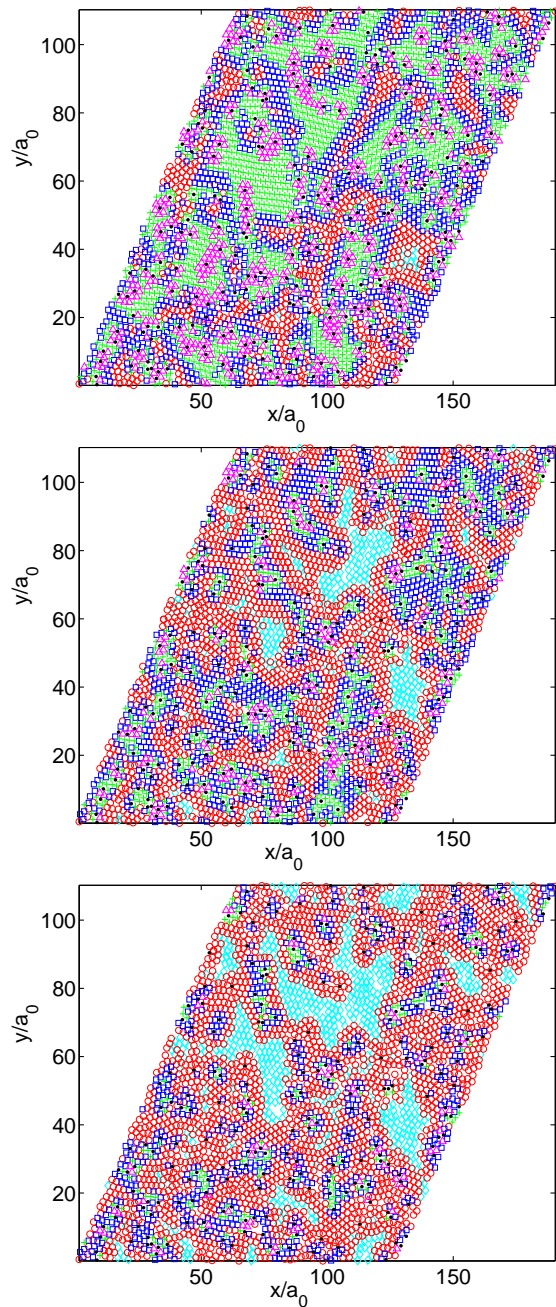


FIG. 8: (Color online). Peak density plots for a sample with $c = 1/16$ (the same sample as in the top left panel of Fig. 7) at temperatures (from top left to bottom) $T = 17.6\text{K}$, $T = 18.4\text{K}$ and $T = 19.2\text{K}$. The locations of the peaks (see text) are displayed as data points, while the values of the density at these peaks are shown according to the (color and) symbol coding: (cyan) diamonds: peaks with $\rho_{\text{peak}}/\rho_0 < 1.5$, (red) empty circles: $1.5 \leq \rho_{\text{peak}}/\rho_0 < 3.5$, (blue) squares: $3.5 \leq \rho_{\text{peak}}/\rho_0 < 5.5$, (green) plus signs: $5.5 \leq \rho_{\text{peak}}/\rho_0 < 7.5$, and (magenta) triangles: $7.5 \leq \rho_{\text{peak}}/\rho_0 < 9.5$. The (black) asterisks denote the positions of pinning centers.

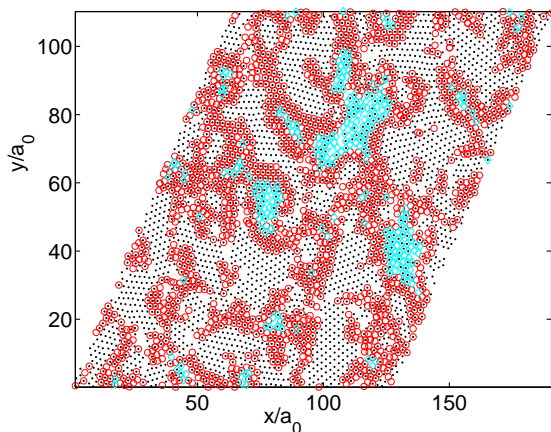


FIG. 9: (Color online) Relation between topological defects and the value of the density peaks. The black dots mark the locations of sixfold coordinated density peaks. The (cyan) diamonds indicate locations where the peak density is low (less than $1.5\rho_0$) while the open (red) circles represent locations with peak density between $1.5\rho_0$ and $3.5\rho_0$. The temperature is 18.4K, $c = 1/16$ and the sample is the same as in Fig. 7 and Fig. 8.

in a liquid state. At the lowest temperature displayed, one can see rather large regions where the vortices are indeed strongly localized. These regions are separated by smaller regions where the vortices are more delocalized. By comparing this figure (in particular the top right panel) with the top left panel of Fig. 7, one sees that the delocalized regions are associated with high defect density, indicating that the vortices lying near the grain boundaries are more delocalized than the ones lying inside the crystalline grains. It is apparent that, as T increases, the regions with higher values of $\rho_{\text{peak}}/\rho_0$ shrink, as the localized, more solid-like, regions “melt” into more liquid-like areas. One can visualize, therefore, that the ongoing transition process proceeds very locally, with different regions in the sample behaving in different ways. This explains the very rounded “transition” observed in the order parameter and free energy plots (Figs. 6 and 5 respectively).

There is another way to observe the correlation between the defect structure and the values of the local peak density in the vortex lattice, and this view is shown in Fig. 9. There we consider again $c = 1/16$ at $T = 18.4\text{K}$. This plot combines features of Figs. 7 and 8. The same sample as in Fig. 8 is considered. The six-fold coordinated peak locations only (that is, the ones not associated with defects) are shown as black dots, while only the peak positions with low values of the peak density are indicated by the symbol (and color) scheme. One can then clearly notice that the local density peaks with low values of the peak density are mostly associated with peak positions that are *not* six-fold coordinated. This plot clearly illustrates the strong correlation between the degree of localization and the presence of topological defects: vor-

tices lying near grain boundaries where the topological defects are concentrated are more delocalized than the ones lying inside the crystalline grains. A similar correlation between the degree of localization and the presence of defects has been observed in several experimental and numerical studies of particle systems³¹.

The question still remains, of how to characterize the smooth “transition” between BoG and IL phases for $c \geq 1/16$. Since the minimum representing the IL at high temperatures transforms continuously into the one corresponding to the BoG phase at low temperatures, we can not use a crossing of free energies to locate the transition temperature, as was done for smaller values of c . We are here guided by two observations: one is that the transition is so broad because it takes place locally at different temperatures in different regions of the sample. Second, it was noted in Ref. 20 that at lower concentrations, the BoG to IL melting transition coincides with a percolation process: at lower T the solid-like regions percolate throughout the sample, while at higher T it is the liquid-like regions that do. It was also noted there that one can define a local transition temperature using a criterion based on the degree of localization of the vortices, that this local transition temperature varies across each sample, and that the temperature at which regions that have already melted percolate across the sample coincides with the global transition temperature determined from the crossing of the free energies of the minima representing the two phases. A similar connection between the BoG–IL transition and percolation is suggested in a numerical study²⁵ of a disordered two-dimensional boson model to which the thermodynamic behavior of the system under study here can be mapped approximately.

We adopt here then this point of view and search for a percolation transition. At concentrations larger than $c = 1/32$, the temperature at which this transition occurs is then plotted as the dashed melting curve of Fig. 1. Two examples of our search for percolation are shown in Fig. 10. Two samples are considered, one at $c = 1/16$ the other at $c = 1/8$. In the plots we identify the local density peak sites where $\rho_{\text{peak}}/\rho_0 \leq 3$ as being in a liquid region, and those for which $\rho_{\text{peak}}/\rho_0 > 3$ as belonging to a solid-like region. This criterion was found²⁰ to be appropriate in our studies of systems with smaller values of c . We can see in Fig. 10 that a percolation transition can indeed be located, and that the transition temperature increases with c . The results are remarkably consistent across samples of the same concentration. The results used to plot this portion of the phase boundary (dashed line) in Fig. 1 are averages over three to five samples.

A local transition temperature can also be defined and the results correlated with the percolation plot. To do this we divide the vortex lattice into small regions containing about 16 vortices each. Within these regions we can calculate the average local peak density, ρ_{av}^p . In calculating this average, we exclude the very high peaks associated with any existing pinning centers. The “local melting temperature” of each of the small regions is

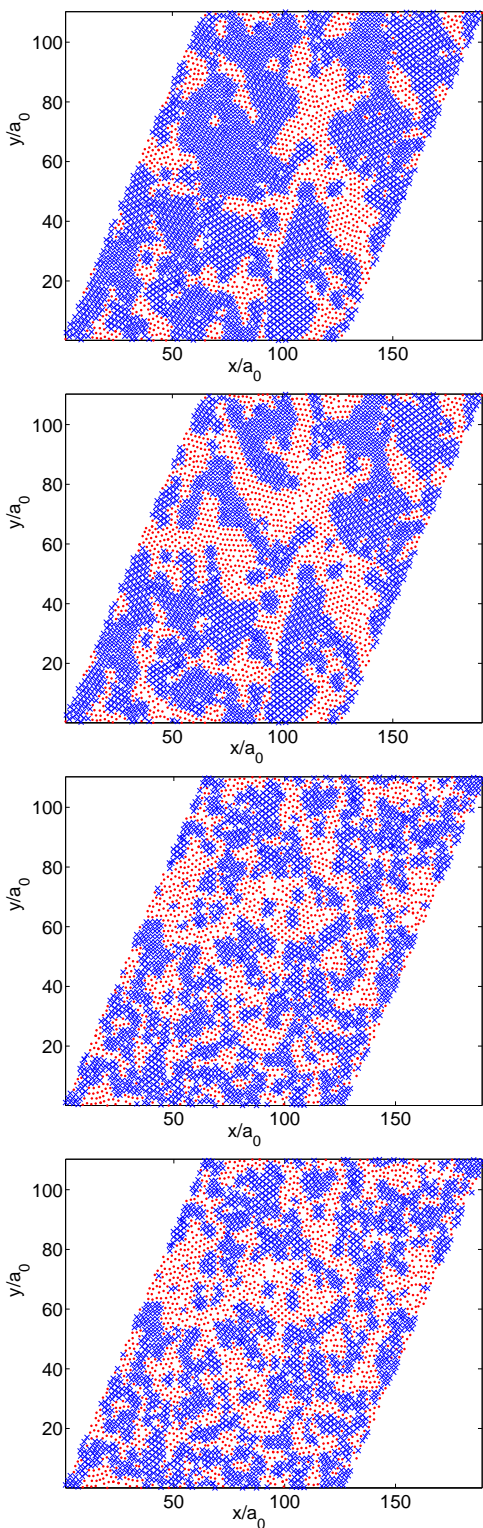


FIG. 10: (Color online) Percolation plots. The (blue) crosses represent regions where the system is solid-like (see text) while the (red) dots indicate liquid-like areas. The two top panels are for $c = 1/16$ at $T = 18.2\text{K}$ (left side, where the solid percolates) and $T = 18.4\text{K}$ (right side, where the liquid percolates). The two bottom panels are for $c = 1/8$ and $T = 19.8\text{K}$ (left) and $T = 20.0\text{K}$ (right).

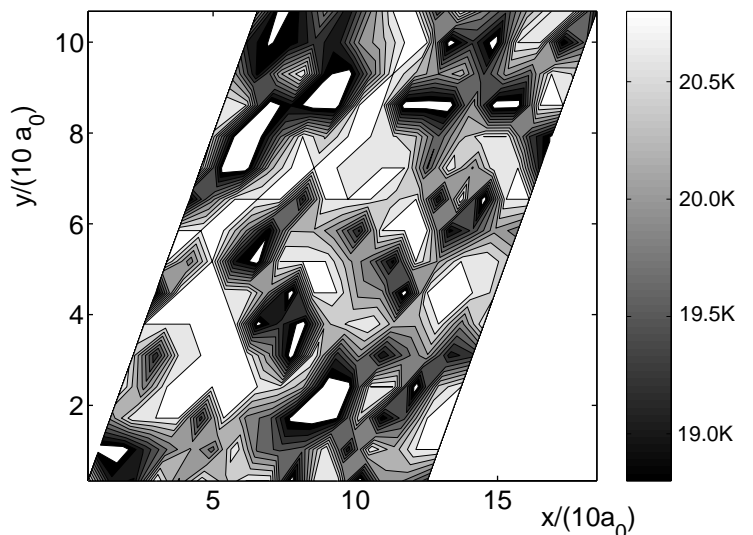


FIG. 11: Gray scale (as indicated) contour plot of the local melting temperature as defined in the text. Results shown are for one sample with $c = 1/8$ where percolation occurs near $T = 20\text{K}$.

then defined as the temperature at which ρ_{av}^p for that particular region drops (as the overall T increases) from above the threshold value of $3\rho_0$ discussed above, to below. An example is shown in Fig. 11, for a concentration $c = 1/8$ in the upper limit of the range studied. This is a gray scale plot in which the values of this local melting temperature are shown according to the code indicated by the adjacent bar. Similar spatial variations of a local transition temperature have been observed in several experiments^{6,23}. For this sample, the overall transition, as determined by the percolation method, occurs at 20K . It is clear from the plot that the regions of the sample that have melted at $T = 20\text{K}$ form a barely percolating cluster, indicating that the result for the transition temperature obtained from these considerations is consistent with that of the overall percolation analysis.

D. Depinning crossover

The above completes the discussion of the main portion of the phase diagram. It remains to explain how the depinning temperature (the dotted line on the right side of Fig. 1) was determined. To discuss this point we begin by noting that at sufficiently low T , every pinning site should hold one vortex. Indeed, as explained above, the strength and range of the pinning potential were chosen so that this would be the case. One can verify that this is so by adding, for a given pinning center, the values of the variables ρ_i on the computational lattice, for all the sites i which are within the pinning range r_0 of that pinning center. This “integrated density” at a pinning center²⁴ is nothing but the time averaged number of vortices pinned at that center. At low T it tends to unity at nearly all

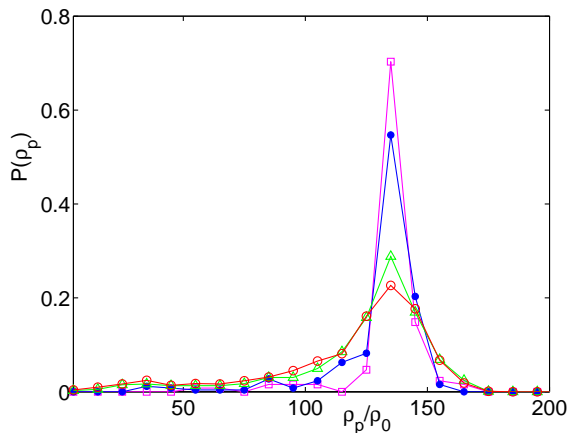


FIG. 12: (Color online). Distribution of the peak density ρ_p (see text) evaluated at each computational cell containing a pinning center for different values of c . The vertical axis is the probability of having a certain value of the normalized ρ_p . Results are shown at $T = 21.6\text{K}$ for four different concentrations: $c = 1/64$ [(magenta) squares], $c = 1/32$ [(blue) filled circles], $c = 3/32$ [(green) triangles], and $c = 1/8$ [(red) open circles]. Straight solid lines join successive data points

centers, the rare exceptions occurring in some configurations at high c where two sites may be very close to each other.

For a given configuration, we can similarly compute for each pinning center a quantity ρ_p , defined as the vortex density in a computational cell that contains a pinning center ($\rho_p \equiv \rho_i / (\sqrt{3}h^2/2)$ where ρ_i is the discrete density variable at computational cell i which contains a pinning center, and h is the spacing of the computational mesh). This quantity should not to be confused with ρ_{peak} which refers to the density at local density peaks other than the ones at pinning centers. It is very instructive to consider the distribution of ρ_p values (normalized to ρ_0) as a function of c and T . Such distributions for several different values of c at a fixed $T = 21.6\text{K}$, near the depinning temperature, are shown in Fig. 12. These distributions are sharply peaked at a value which is somewhat less than that corresponding to having one vortex in the cell (one vortex in a computational cell corresponds to a value of about 234.9 for the normalized quantity ρ_p/ρ_0), regardless of c . The distribution broadens markedly with increasing c and a small secondary peak on the low side develops. At these values of T and c , the percentage of pinning sites that hold only a small fraction of a vortex is clearly not negligible.

This behavior can be understood from a consideration of the effects of neighboring pins on the probability of a particular pinning center being occupied by a vortex. Due to the strong short-distance repulsive interaction between two vortices, two pinning centers that lie very close to each other can not be simultaneously occupied. As shown in Ref. 24, this interaction effect becomes important when the separation between two pinning centers

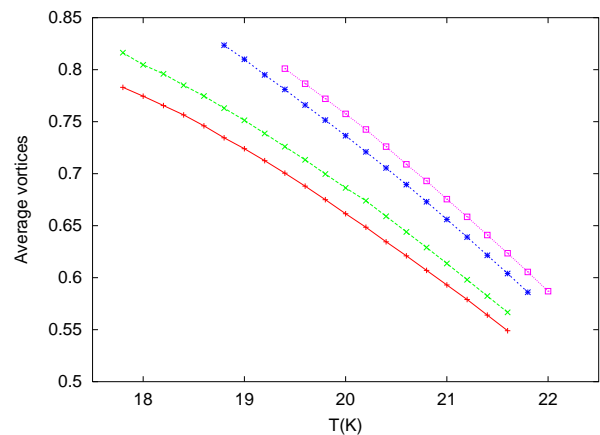


FIG. 13: (Color online) The average number of vortices pinned at each pinning center, as a function of T , for four values of c : (red) plus signs and solid line are for $c = 1/8$, (green) crosses and long dashed line, $c = 3/32$, (blue) asterisks and short dashes, $c = 1/32$, (magenta) squares and dotted line, $c = 1/64$.

becomes smaller than about half the average intervortex spacing. Specifically, it was shown there that for values of B , T and the pinning parameters α and r_0 very similar to those used in the present calculation, two pinning centers separated by less than a_0 are not simultaneously occupied. We find that all the pinning centers for which the value of ρ_p/ρ_0 is less than 50 have at least another pinning center within a distance a_0 from them. The probability of finding such closely spaced pairs of pinning centers obviously increases with increasing c . This is the reason for the broadening of the distribution of ρ_p/ρ_0 on the low side as c is increased. The pinning efficiency of a pinning center can also be enhanced by the presence of a neighboring pin if the distance between the two pins is close to the average intervortex spacing²⁴. This is the reason for the occurrence of the tail of the distribution of ρ_p/ρ_0 on the high side. However, the overall effect is a reduction in the average value of ρ_p/ρ_0 as the pin concentration is increased.

The integrated density at each pinning center can be averaged over all centers, and also over all pin configurations at a given value of c and T to obtain an overall average number of vortices pinned at each pinning center at that concentration and temperature. This is of course the quantity of main interest to determine the overall behavior of the system. Results for this average number of vortices are plotted in Fig. 13 as a function of temperature, for several concentrations. The results are averages over four or five samples, the dispersion being very small. At low T the average number of vortices tends towards unity, and it decreases as T increases. It is in general (see Fig. 13) a function of c , decreasing as c increases. This reflects the interaction effects discussed above and depicted in Fig. 12. In Ref. 24 it was shown (see Fig. 3 of that work) that the average number of vortices pinned by

a single center, as a function of the strength parameter α at constant T , increases sharply from a low value to one close to unity as the value of α increases, with the middle of this sharp increase occurring at a value corresponding to the integrated density being close to 0.6. It is therefore appropriate to associate the depinning temperature with the point where each curve in Fig. 13 crosses the “critical” value of 0.6, and this criterion has been used to determine the location of the depinning line in Fig. 1. This criterion is very similar to the one used in Ref. 12 where the effects of other pinning centers on the pinning properties of a particular one were not considered. Consequently, Ref. 12 predicts a depinning temperature that is independent of c for a fixed value of B . The small reduction of the depinning temperature with increasing c seen in Fig. 1 reflects the interaction effects discussed above, which reduce the pinning efficiency of individual pinning centers as c is increased.

The depinning temperature has been experimentally measured⁸ in samples of BSCCO for several small concentrations of columnar pins. It is found that the depinning temperature for fixed B in the regime where the depinning crossover occurs in the liquid state (the regime considered in our calculations) is rather insensitive to the pin concentration c . This is in qualitative agreement with our results. There is, however, a small discrepancy: the experimental results³² show a small increase of the depinning temperature with increasing c , whereas we find a small decrease. This difference may be understood as arising from the different criteria used to define the depinning crossover, in the following way.

In the experiment⁸, the depinning temperature is determined from the difference between the transport currents in the pristine (without columnar pins) and irradiated (with columnar pins) regions of the sample. This difference arises because the pinning property of the IL (which is found only in the irradiated parts of the sample) with both liquid- and solid-like regions is different from that of the homogeneous vortex liquid that exists in the pristine parts of the sample. Now, our study shows that solid-like regions in the IL occur near clusters of columnar pins (see, e.g. Fig. 3 of Ref. 20). The pinning property of such a solid-like region depends both on the pinning efficiency of individual pins, and on the size (number of pins) of the cluster of pins present in the region. The average cluster size increases with increasing c . So, it is reasonable to expect that the pinning efficiency of a typical solid-like region in the IL would also increase with c . Also, the fraction of solid-like regions in the IL at a fixed temperature would be higher for larger values of c . These considerations imply that the pinning properties of the inhomogeneous IL would become similar to those of the homogeneous liquid at a higher T in samples with larger c . Thus, this effect tends to increase the delocalization temperature obtained from the current distribution as c is increased. It may dominate over the small decrease arising from the effect found in our calculation, thereby producing an overall increase in the measured delocaliza-

tion temperature as the value of c is increased. A similar argument would also explain the differences between our results for the depinning line and those obtained in the simulations of Nonomura and Hu¹⁶ who used the measured value of the tilt modulus to determine the depinning temperature. Since the depinning is a crossover, not a thermodynamic phase transition, it is not surprising that different criteria lead to slightly different results for the depinning temperature.

IV. SUMMARY AND DISCUSSION

We have reported here the results of a detailed investigation of the phase diagram of a highly anisotropic layered superconductor with columnar pinning in the temperature (T) – pin concentration (c) plane. For small values of c , we confirm the occurrence^{19,20} of a topologically ordered BrG phase at low temperatures and a two-step first-order melting of the BrG phase into an IL, with a small region of intermediate polycrystalline BoG phase. In the IL, a fraction of vortices remains localized at the strong pinning centers. The IL crosses over into a completely delocalized vortex liquid at a depinning temperature that is higher than the temperature at which the BoG–IL transition occurs. The BrG phase disappears as the pin concentration is increased and the two-step melting found at low pin concentrations is replaced by a single continuous transition from a low-temperature BoG phase to a high-temperature IL. This transition corresponds to the onset of percolation of liquid-like regions across the system. The temperature at which this percolation transition occurs increases with increasing pin concentration, while the depinning temperature is nearly independent of the pin concentration. Consequently, the width of the temperature interval in which the IL is found decreases and eventually goes to zero when the pin concentration becomes sufficiently high (slightly above 1/8).

Although the system we have considered here is three dimensional, since we do take into account the electromagnetic interaction between vortices on different layers, the correlated nature of the pinning produced by the columnar defects makes it, in some sense, quasi two dimensional. The presence of a BrG phase in our phase diagram may then appear surprising in view of the well-known result³³ that a BrG phase does not exist in two dimensions. It has been argued³⁴ that a BrG phase is unlikely to exist in a three dimensional system with columnar pins. From our study of finite-size samples, we can not, of course, rule out the possibility that for any non-zero value of the pin concentration c , disorder-induced free dislocations would appear at length scales much larger than those accessible in our study. It is, however, very clear from our results (see results above and also Refs. 19,20) that the structure of the nearly crystalline minima we have found for small c is qualitatively different from that of the polycrystalline BoG minima found for the same values of c . Thus, our conclusion

about the occurrence of a first-order phase transition between the polycrystalline BoG phase found near the melting transition and a much more ordered phase found at low temperatures for small c would remain valid even if the nature of the nearly crystalline phase turns out to be different from a true BrG.

Several noteworthy features found in our study have been observed in experiments^{5,6,7,8} on BSCCO with small concentrations of random columnar pins: Thus, our findings of the polycrystalline nature of the low-temperature BoG phase for small pin concentrations; the existence of the IL (called “vortex nanoliquid” in Ref. 8) with a coexistence of pinned and delocalized vortices, which crosses over into a fully delocalized vortex liquid at a “depinning” temperature; the existence of a first-order transition between the IL and BoG phases for small values of c , which becomes continuous as c is increased keeping B constant; the increase of the BoG–IL transition temperature with increasing pin concentration; and the spatial variations of a locally defined transition temperature, all are in agreement with experimental results. Our results are also similar to those obtained in the simulation of Ref. 16, except for some small differences in the location of the depinning line which, as discussed in section III D, may be attributed to the use of different criteria for determining the temperature at which the depinning crossover occurs. The low-temperature BrG phase found here for small c has not yet been observed in experiments. As discussed in Ref. 20, this may be due to the metastability of the BoG phase into which the vortex liquid freezes as the temperature is decreased in the presence of a magnetic field. Explorations of ways in which this metastability can be avoided would be worthwhile. We note that a recent study³⁵ of grain boundaries in vortex matter suggests that the melting of the vortex lattice in unpinned systems can also be preceded by an intermediate polycrystalline phase.

Our computations have been performed for a fixed value of the magnetic induction, $B = 2\text{kG}$. The behavior of the system for other values of B may be inferred from our results by combining them with those of other existing studies^{28,38,39}. As discussed in section III C, we find that for fixed B the number of crystalline domains in a polycrystalline BoG minimum is proportional to the pin concentration c . This suggests that the typical size of the crystalline domains is determined primarily by the arrangement of the pinning centers. If this is so then for a fixed arrangement of the pinning centers, the typical number of vortices lying inside a crystalline grain would be proportional to B . This is precisely as observed in the above mentioned experiments of Ref. 7. Earlier studies²⁸ of the model of pancake vortices considered here indicate that interlayer vortex correlations decrease as B is increased and the system becomes effectively two-dimensional (the melting temperature of the pure vortex lattice approaches that of the two-dimensional system) in the limit of large B . Existing studies^{38,39} of the ground states (or low-lying local minima of the energy)

of randomly pinned two-dimensional vortex arrays show polycrystalline structures similar to those found for the BoG phase in our work. We therefore expect that the polycrystalline structure of the BoG phase would remain essentially unchanged as B is increased for a fixed concentration of pinning centers. Since the melting temperature of the pure vortex lattice decreases²⁸ with increasing B , the temperature at which the BoG–IL transition occurs would be expected to decrease as B is increased at constant pin concentration. Existing results³³ about the absence of a true Bragg glass in two dimensions suggest that the BrG phase found for small c in our study would not be present in the effectively two-dimensional large- B limit.

Numerical studies^{16,40} in which the vortex system is represented by a frustrated XY model do not find any clear evidence for the formation of polycrystalline structures, whereas all existing numerical studies^{14,38,39} in which the vortices are modeled as interacting particles (or lines) indicate that the structure of the low-temperature disordered phase is polycrystalline, as found in our study. The reason for this difference is not clear. It may be due to the smallness of the sample sizes (~ 100 vortex lines in the simulation of Ref. 16) used in the studies based on the frustrated XY model. A polycrystalline structure can be discerned clearly if the crystalline grains are large enough (e.g. for $c = 1/64$ and $1/32$ in our calculation). Such large grains would be observed in a simulation only if the sample size is much larger than the typical grain size, which is probably not the case in the simulations of Refs. 16,40 for weak pinning. For stronger pinning, the typical grain size would become smaller than the sample sizes considered in these studies. However, in this limit, it would be difficult to distinguish a polycrystalline structure from an amorphous one. This difficulty should be clear from an inspection of a small part (containing ~ 100 vortices) of the bottom panel of Fig. 7 (for $c = 1/8$) for which the grain size is small.

Quantitatively, this mean-field calculation is expected to provide accurate results for the transition temperatures as long as the transitions are strongly first-order. This is true for the transitions that occur at small values of c in our phase diagram. Our predictions are quantitatively less reliable for larger values of c for which the transition is continuous. The method of locating the transition temperature from the crossing of the free energies of different local minima of the free energy does not work when the transition is not first-order. Strictly speaking, the alternative method of identifying the transition point as the temperature at which liquid-like regions percolate across the system cannot conclusively determine whether there is a true continuous transition for large c , or just a crossover from a high-temperature liquid-like state to a low-temperature frozen state. We assume that a continuous BoG–IL transition occurs in this regime because such a transition is found in transport experiments and in numerical work in which the superconducting phase variables are included. These aspects are not accessible

in our work because the free energy we consider involves only the local density of the vortices. However, we believe that our estimate of the BoG–IL transition temperature from the percolation criterion we have used is reliable. The reason for this assertion is that a similar criterion works quantitatively well for the continuous transition in disordered two-dimensional boson models to which the vortex problem we consider here can be mapped. Also, transitions between liquid and glassy phases in several other systems, such as colloidal systems³⁶ and thin polymeric films³⁷, have been quite satisfactorily described in the past in terms of percolation criteria similar to the one

used here. It would be interesting to test the validity of this description of the BoG–IL transition in experiments in which magneto-optic techniques^{6,8} can be used to map out the local liquid- or solid-like character of different regions of the sample.

V. ACKNOWLEDGMENTS

One of us (C.D.) wishes to thank S. Banerjee, X. Hu, T. Nattermann and E. Zeldov for helpful discussions.

-
- * cdgupta@physics.iisc.ernet.in; Also at Condensed Matter Theory Unit, Jawaharlal Nehru Centre for Advanced Scientific Research, Bangalore 560064, India.
- † otvalls@umn.edu
- ¹ L. Civale, A. D. Marwick, T. K. Worthington, M. A. Kirk, J. R. Thompson, L. Krusin-Elbaum, Y. Sun, J. R. Clem, and F. Holtzberg, *Phys. Rev. Lett.* **67**, 648 (1991).
 - ² R.C. Budhani, M. Suenaga and S. H. Liou, *Phys. Rev. Lett.* **69**, 3816 (1992).
 - ³ R. C. Budhani, W. L. Holstein and M. Sunega, *Phys. Rev. Lett.* **72**, 566 (1994).
 - ⁴ W. Jiang, N.-C. Yeh, D. S. Reed, U. Kripalni, D. A. Beam, M. Konczykowski, T. A. Tombrello, and F. Holtzberg, *Phys. Rev. Lett.* **72**, 550 (1994).
 - ⁵ B. Khaykovich, M. Konczykowski, K. Teitelbaum, E. Zeldov, H. Shtrikman and M. Rappaport, *Phys. Rev.* **B57**, R14088 (1998).
 - ⁶ S. S. Banerjee, A. Soibel, Y. Myasoedov, M. Rappaport, E. Zeldov, M. Menghini, Y. Fasano, F. de la Cruz, C. J. van der Beek, M. Konczykowski, and T. Tamegai, *Phys. Rev. Lett.* **90**, 087004 (2003).
 - ⁷ M. Menghini, Yanina Fasano, F. de la Cruz, S. S. Banerjee, Y. Myasoedov, E. Zeldov, C. J. van der Beek, M. Konczykowski, and T. Tamegai, *Phys. Rev. Lett.* **90**, 147001 (2003).
 - ⁸ S. S. Banerjee, S. Goldberg, A. Soibel, Y. Myasoedov, M. Rappaport, E. Zeldov, F. de la Cruz, C. J. van der Beek, M. Konczykowski, T. Tamegai, and V. M. Vinokur, *Phys. Rev. Lett.* **93**, 097002 (2004).
 - ⁹ D. R. Nelson and V. M. Vinokur, *Phys. Rev. B* **48**, 13060 (1993).
 - ¹⁰ L. Radzihovsky, *Phys. Rev. Lett.* **74**, 4923 (1995).
 - ¹¹ A. I. Larkin, and V.M. Vinokur, *Phys. Rev. Lett.* **75**, 4666 (1995).
 - ¹² A. V. Lopatin and V. M. Vinokur, *Phys. Rev. Lett.* **92**, 067008 (2004).
 - ¹³ R. Sugano, T. Onogi, K. Hirata, and M. Tachiki, *Phys. Rev. Lett.* **80** 2925 (1998).
 - ¹⁴ P. Sen, N. Trivedi, and D. M. Ceperley, *Phys. Rev. Lett.* **86**, 4092 (2001).
 - ¹⁵ S. Tyagi and Y. Y. Goldschmidt, *Phys. Rev. B* **67**, 214501 (2003).
 - ¹⁶ Y. Nonomura and X. Hu, *Europhys. Lett.* **65**, 533 (2004).
 - ¹⁷ Y. Y. Goldschmidt, *Phys. Rev. B* **56**, 2800 (1997).
 - ¹⁸ T. Giamarchi and P. Le Doussal, *Phys. Rev. B* **52**, 1242 (1995).
 - ¹⁹ C. Dasgupta and O.T. Valls, *Phys. Rev. Lett.* **91**, 127002 (2003).
 - ²⁰ C. Dasgupta and O.T. Valls, *Phys. Rev. B* **69**, 214520 (2004).
 - ²¹ T.V. Ramakrishnan and M. Yussouff, *Phys. Rev. B* **19**, 2775 (1979).
 - ²² The free-energy minima we identify as representing the BrG phase exhibit BrG-like properties over the length scales accessible in our samples of finite size.
 - ²³ A. Soibel, Y. Myasoedov, M. L. Rappaport, T. Tamegai, S. S. Banerjee, and E. Zeldov, *Phys. Rev. Lett.* **87**, 167001 (2001).
 - ²⁴ C. Dasgupta and O.T. Valls, *Phys. Rev. B* **66**, 064518 (2002).
 - ²⁵ K. Sheshadri, H. R. Krishnamurthy, R. Pandit and T. V. Ramakrishnan, *Phys. Rev. Lett.* **75**, 4075 (1995).
 - ²⁶ C. Dasgupta and D. Feinberg *Phys. Rev. B* **57**, 11730 (1998).
 - ²⁷ See e.g. J.P. Hansen and I.R. McDonald, *Theory of simple liquids*, (Academic, London, 1986).
 - ²⁸ G. Menon, C. Dasgupta, H.R. Krishnamurthy, T.V. Ramakrishnan, and S. Sengupta, *Phys. Rev. B* **54**, 16192 (1996).
 - ²⁹ C. Dasgupta, *Europhysics Lett.* **20**, 131 (1992).
 - ³⁰ P. Kim, Z. Yao, and C. M. Leiber, *Phys. Rev. Lett.* **77**, 5118 (1996).
 - ³¹ R. P. A. Dullens and W. K. Kegel, *Phys. Rev. E* **71**, 011405 (2005), and references therein.
 - ³² E. Zeldov and S. Banerjee, private communication.
 - ³³ C. Zeng, P. L. Leath and D. S. Fisher, *Phys. Rev. Lett.* **82**, 1935 (1999).
 - ³⁴ T. Giamarchi and P. Le Doussal, *Phys. Rev. B* **55**, 6577 (1997).
 - ³⁵ P. Moretti, M. Carmen Miguel and S. Zapperi, cond-mat/0412437.
 - ³⁶ E. R. Weeks, J. C. Crocker, A.C. Levitt, A. Schofield, and D. A. Weitz, *Science* **287**, 627 (2000).
 - ³⁷ A. R. C. Baljon, J. Billen, and R. Khare, *Phys. Rev. Lett.* **93**, 255701 (2004).
 - ³⁸ Mahesh Chandran, R. T. Scalettar and G. T. Zimanyi, *Phys. Rev. B* **69**, 024526 (2004).
 - ³⁹ S. S. Ghosh and C. Dasgupta, manuscript in preparation.
 - ⁴⁰ J. P. Rodriguez, *Phys. Rev. B* **70**, 224507 (2004).